

Frequency Up-Shift in the Interaction of High Power Microwave with Underdense Inhomogeneous Plasma

XU Xiaoxi, NISHIDA Yasushi and YUGAMI Noboru

*Department of Electrical and Electronic Engineering, Utsunomiya University,
Tochigi 321, Japan*

(Received 31 July 1995/Revised manuscript: received 13 September 1995)

Abstract

The frequency up-shifts around several megahertz and other higher frequency components have been observed in the interaction of a high power microwave with an unmagnetized inhomogeneous argon plasma, while there is no ionization front in the present experiments. The dependencies of the up-shifts and higher frequency components on plasma density, incident microwave power and spatial position have been clearly demonstrated in our experiments. The time evolution of these frequency components has also been investigated. The observed frequency up-shifts are considered to be related to a rapidly expanding plasma which is created by the ponderomotive force of a strong standing wave due to the incident microwave. The theoretical calculations have been carried out, and the results are in fairly good agreement with the results observed in the present experiments.

Keywords:

frequency up-shift, frequency down-shift, Stokes line, ponderomotive force, moving plasma, standing wave, Doppler effect, ionization front, Lorentz transformation

1. Introduction

The frequency shift is one of very important topics for plasma physics and new high power microwave source. Such as in laser-driven inertial-confinement fusion (ICF), a pump wave may couple to an acoustic photon and an electromagnetic wave (Stimulated Brillouin Scattering: SBS) so that a frequency down-shift of the scattered electromagnetic wave can be observed [1,2]. This phenomenon is a significant concern for laser fusion applications, since the process can either decrease the amount of energy absorbed or decrease the implosion symmetry [3,4]. The frequency up-shifts, because of their potentiality to develop high power radiation sources, have been studied extensively in laser plasma interaction [5,6,7]. For example, plasma simulation studies [5] indicate that frequency up-shifts may be resulted when a laser pulse interacts with a plasma-wave wake field which has a phase velocity near the

speed of light. Theoretical analysis [6,7] also shows that when a laser pulse propagates in the region of an ionization front in which the local density gradient is negative, it will be continuously up-shifted in frequency. This mechanism has first been observed as a frequency self-up-shifted of an ionizing laser pulse [8], and the use of laser-produced ionization fronts [9,10] have up-shifted a microwave radiation from 30GHz to over 150GHz successfully [11,12]. In these experiments, the ionization fronts play a very important role in frequency up-shifts. It is also found that large frequency up-shifts can be obtained even by underdense relativistic ionization fronts [10,12], where the incident radiation is transmitted into the plasma.

In this paper, we present experimental results where high power pulsed microwaves are launched into an unmagnetized underdense argon plasma. The frequency spectra of the microwaves have been

investigated, the frequency up-shifts around 2MHz and some other higher frequency components from 3MHz to 23MHz have been observed. Because no ionization front is found in the present experiments, this new phenomenon is thought to be related to a rapidly expanding plasma which is created by the ponderomotive force arising from a standing wave. When the incident microwave interacts with a plasma moving at a very high speed, the frequency is then up-shifted due to Doppler effect.

The organization of the present paper is as follows. In Section 2 we describe the experimental apparatus and measurement methods. The experimental results are given in Sec. 3. Theoretical model is presented in Sec. 4. Finally, Sec. 5 contains a summary of the principle conclusions of this work.

2. Experimental Set-Up and Methods

The apparatus used in the present experiments is shown schematically in Fig. 1(a). A cylindrical, azimuthally symmetric, unmagnetized argon plasma column is created in a vacuum chamber (32cm in diameter, 60cm in length). The outside surface of the vacuum chamber is covered with a large number of multidipole permanent magnets (cusp spacing ≈ 4 cm) for the confinement of the primary ionizing electron. The plasma is produced by a pulsed DC discharge between two directly heated LaB₆ cathodes and the chamber wall (grounded). The spiral shaped LaB₆ cathodes used in the present experiments are 10mm in diameter and 25mm in length. The work function is $\phi \approx 2.7$ eV and the operating temperature is about 1670~1920K°. Argon gas is introduced into the chamber by a needle

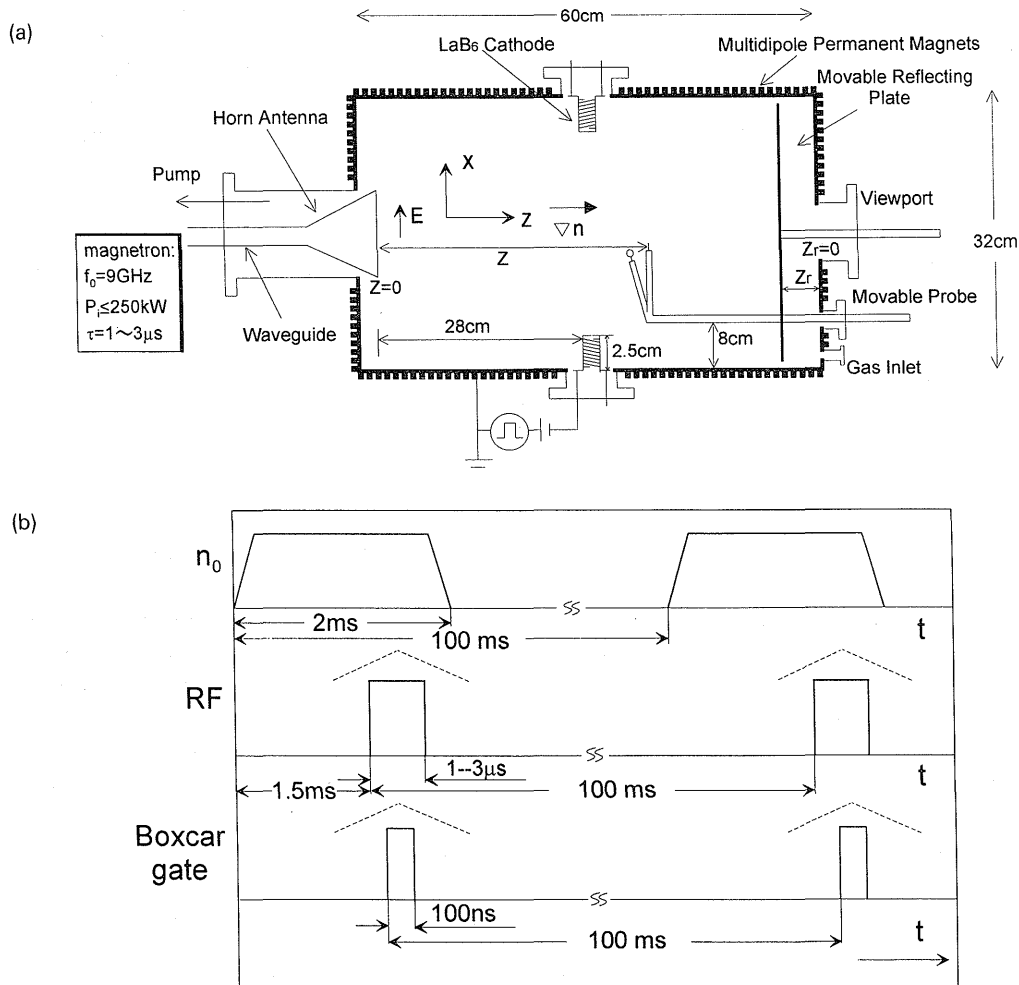


Fig. 1 (a) Experimental setup. Typical parameters are: $f_0=9$ GHz, $P_i \leq 250$ kW, $\tau \approx 1 \sim 3$ μ s, $\epsilon_0 E_0^2 / 4n_e K T_e \approx 0.1$. Assume at the aperture of the horn antenna $z=0$ and at the end wall of the chamber $z_r=0$. (b) Experimental pulse sequences.

valve. The base pressure P_0 of the chamber is $P_0=2 \times 10^{-6}$ Torr and neutral fill pressure P_{Ar} is typically $P_{Ar}=2 \times 10^{-3}$ Torr. A typical plasma discharge pulse duration is $t_w \approx 2$ ms and a usual discharge voltage is 150V, with a repetition rate of 10Hz. The plasma density is measured by both cylindrical and plane Langmuir probes. A pulsed microwave radiation ($f_0=9$ GHz) with a maximum rise-time $\tau_r \approx 100$ ns and a pulsewidth of $\tau \approx 1 \sim 3 \mu$ s is generated by a magnetron with a repetition rate of 10Hz. The microwave is injected into the plasma synchronously with the discharge pulse through a rectangular horn antenna (aperture area= 13.5×10.5 cm²) from the lower density side of the plasma along the chamber axis (z direction). The experimental pulse sequences are shown in Fig. 1(b). A moveable reflecting plate (30cm in diameter) is put at the end of the chamber (at the end wall of the chamber, $z_r=0$) for changing the reflection position of the microwave. The microwave signal is picked up by a moveable cylindrical probe. A spatial scan of the pulsed electric field of the incident microwave and the plasma density are taken along the center axis of the chamber. The axial profiles of the electric field intensity $|E|^2$ and the plasma density are shown in Fig. 2. It is obvious that there is an inhomogeneous standing wave set up in the chamber because of the multi-reflection from the plasma and chamber wall. Especially, there are two very high peaks at $z=11$ and 21cm. Within the experimental region of concern, there is a parabolic density profile along the

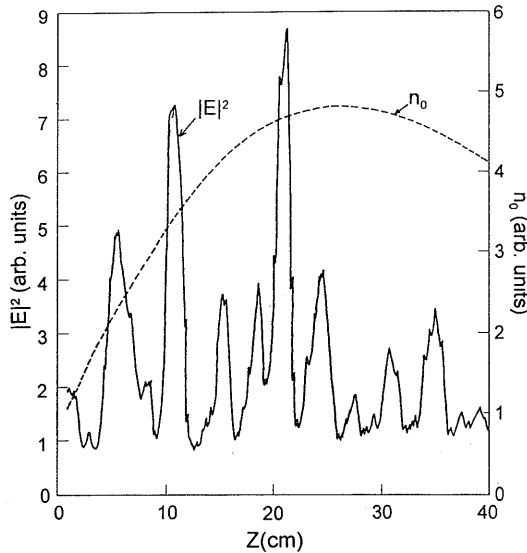


Fig. 2 An example of the axial profiles of the rf electric field intensity and unperturbed plasma density. $f_0=9$ GHz, $P_i=250$ kW, $\tau=1 \mu$ s, $P_{Ar}=2 \times 10^{-3}$ Torr and $z_r=0$.

chamber axis (z direction), $n_0=n_{\max}[1-(z-z_0)^2/L_z^2]$, where L_z is the half-width of the density profile along the chamber axis, n_{\max} is the maximum plasma density and z_0 is the position of the maximum density layer. In the present experiments, the L_z is around 25cm, while L_r , the scale length of the density gradient in radial direction, is around 300cm.

The typical plasma parameters during the discharge are: maximum electron density $n_0 \leq 1.0 \times 10^{12}$ cm⁻³, electron temperature $T_e \approx 3 \sim 5$ eV. The estimated electron-ion collision frequency is $\nu_{ei} \approx 4.5 \times 10^6$ sec⁻¹, and ion neutral collision frequency is $\nu_{in} \approx 10^5$ sec⁻¹. The ratio of the electric field energy to the plasma energy is $\epsilon_0 E_0^2 / 4n_c K T_e \approx 0.1$, where E_0 is the amplitude of the electric field of the incident microwave, $n_c=1.0 \times 10^{12}$ cm⁻³ is the critical plasma density and K is Boltzmann's constant. Because the pulsewidth of the microwave is shorter than the ionization or plasma heating times, and the increment of the plasma density has not been observed when the incident microwave pulse is interacting with the plasma, the effects of the ionization can be safely neglected. The experiments are carried out when there is no critical layer in the chamber, or in the other words, the incident microwave interacts with an underdense plasma. The microwave signals are picked up by the moveable cylindrical probe in the chamber and the frequency spectrum of the microwave is observed by a spectrum analyzer. The observed frequency spectrum of the microwave is recorded by a X-Y recorder connected to a Boxcar amplifier. The plasma density perturbation is detected by a moveable plane Langmuir probe and observed by a digital storage oscilloscope.

3. Experimental Results

3.1. Typical frequency spectra in the plasma

The spectra of rf signals with pulsewidth of $\tau=1$ and 3μ s are observed along the center axis of the chamber, respectively, in the present experiments. The obvious frequency shifts are observed around the two very high peaks of the standing wave (see Fig. 2) at $z=11$, 21cm, respectively. The typical frequency spectra of the microwave pulses with and without plasma in the chamber at $z=21$ cm (a distance between the aperture of the horn antenna and the location of the moveable cylindrical probe, see Fig. 1(a).) are shown in Fig. 3(a) and Fig. 3(b). The dashed and solid lines represent the spectra of rf signals in vacuum and in plasma, respectively. The incident power is 250kW, and plasma density is $n_0 \approx 0.6n_c$. In the vacuum, the high peak of the center frequency ($f_0=9$ GHz) with FWHM (full width at

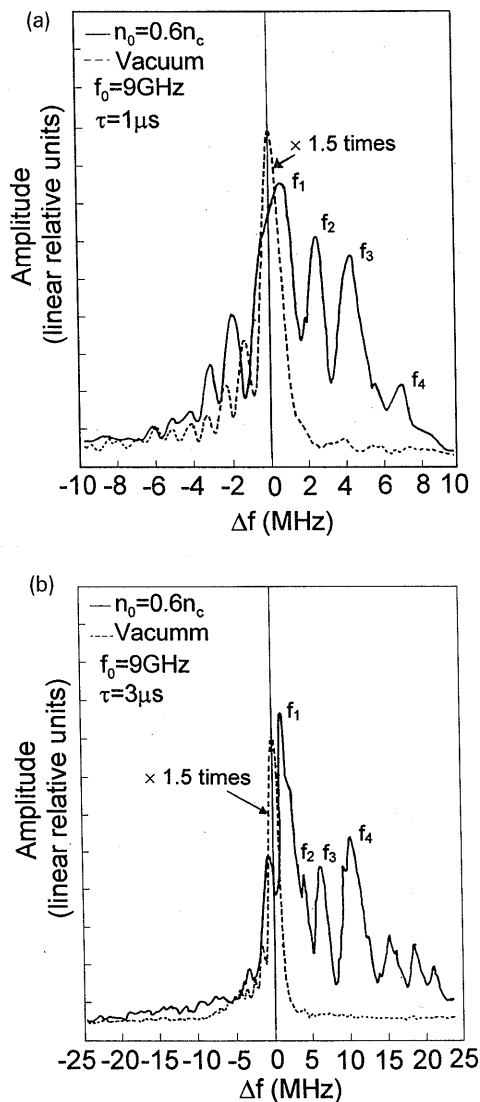


Fig. 3 Frequency spectra of rf signals observed inside the chamber. Dashed line represents the spectrum observed without plasma and solid line shows the case with plasma. Pulse width $\tau=1\mu\text{s}$ for (a), $\tau=3\mu\text{s}$ for (b). $n_0 \approx 0.6n_c$, $n_c=1 \times 10^{12}\text{cm}^{-3}$, $P_i=250\text{kW}$, and $P_{Ar}=2 \times 10^{-3}\text{ Torr}$, $z=21\text{cm}$ and $z_r=0$. Here f_1, f_2, f_3 and f_4 are denoted for convenience.

half maximum) $\approx 2\text{MHz}$ can be seen from Fig. 3. And, it is also noted that several frequency components due to the magnetron appear in the lower frequency range but not in the upper frequency range. In the plasma, the frequency up-shifts (the main peak of the spectra which are denoted by f_1) from the center frequency around 1.0MHz for $\tau=1\mu\text{s}$ and 2MHz for $\tau=3\mu\text{s}$ are demonstrated clearly. As shown in Fig. 3, besides the frequency up-shifts, some new frequency components f_m ($m=2, 3, 4, \dots$) with a continuous frequency back-

ground in upper frequency range have been also observed. Such as $+4, +6, +10, +15, +18,$ and $+21\text{MHz}$ for $\tau=3\mu\text{s}$ can be seen from Fig. 3(b).

In order to investigate the spatial character of the frequency shifts, the cylindrical probe is moved along the center axis of the chamber step by step to detect the frequency spectrum at different positions. As an example, the frequency spectra observed at three different positions, $z=7, 9, 11\text{cm}$, are given in Fig. 4, while the plasma density is $n_0 \approx 0.5n_c$ at $z=11\text{cm}$ and the pulsewidth of the incident microwave τ is $\tau=1\mu\text{s}$. We find that the frequency spectrum of the microwave in the vacuum does not change with the spatial position, but the up-shifted frequency and higher frequency components observed in the plasma are very sensitive to the position where they are observed. The data in Fig. 4 show that the frequency spectra in the plasma have a clear spatial dependence. The frequency up-shift, higher frequency components and their amplitudes are different at each observation position.

As mentioned above, besides the higher frequency components, the lower frequency components can be also seen from the frequency spectra observed in the plasma. But it should note that even in the vacuum, there are Stoke lines in lower frequency range. Furthermore, comparing with amplitudes of the Stokes lines observed in the vacuum, we find that the increment of the amplitudes of the Stokes lines in the lower frequency range which are observed in the plasma is not very obvious. Consequently, we can not confirm that the

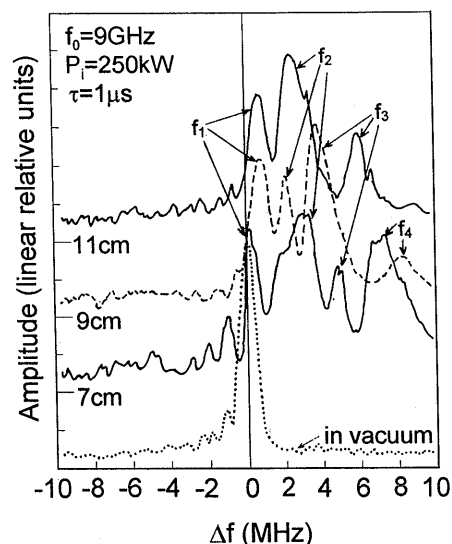


Fig. 4 Spectrum change vs. spatial position z . $n_0 \approx 0.5n_c$ at $z=11\text{cm}$, $P_i=250\text{kW}$, $\tau \approx 1\mu\text{s}$, $P_{Ar}=2 \times 10^{-3}\text{ Torr}$ and $z_r=0$.

observed lower frequency components in the present experiments are from the interaction of the microwave with the plasma or just due to the harmonics created by the magnetron. A theoretical estimation about the amplitudes of the up and down shifted signals are given in Section 4.2. It is also noted that a spectral broadening (continuous background of the spectrum) can be seen from Fig. 3 and Fig. 4. Because a rectangular microwave pulse used in the present experiments and each pulse segment experiences a slightly different frequency shift. And, the scan time of the spectrum analyzer is 50 seconds, so that each recorded spectrum represents an average sampling spectrum of about 500 pulses. This is one of the reasons that continuous spectral broadening can be observed in the present experiments.

3.2. Relationship of frequency spectra and plasma density

For investigating the relation of the frequency up-shifts with the plasma density, we put the plane Langmuir probe and the cylindrical probe at a fixed position, then observe the frequency spectrum while increasing the plasma density gradually. For example, Fig. 5(a) and Fig. 5(b) show the dependence of the frequency spectra on plasma density at a fixed position $z=21\text{cm}$, when incident power $P_i=250\text{kW}$ for $\tau=1, 3\mu\text{s}$, respectively. It can be seen that when the plasma density n_0 is increased from 0 to $0.8n_c$ ($n_c=1 \times 10^{12}\text{cm}^{-3}$) the frequency up-shifts increase slightly around 1.0MHz for $\tau=1\mu\text{s}$, and around 2.0MHz for $\tau=3\mu\text{s}$, while the higher frequency components increase proportionally to the plasma density. The error bar shows the FWHM of every peak of the frequency component. As shown in Fig. 5(a), the frequency of f_2 shifts from 1.3MHz to 4.5MHz, and the frequency of f_3 shifts from 4.0MHz to 6.5MHz. In the case of $\tau=3\mu\text{s}$ which is shown in Fig. 5(b), f_2 increases from 2 to 7MHz and f_3 around 9MHz appears when $n_0 \geq 0.6n_c$.

3.3. Relationship between frequency spectra of the incident power

The relationship between the frequency up-shifts and the incident power of the microwave has also been investigated. The spectrum is observed at a fixed point with the plasma density keeping unchanged. The two typical frequency spectra observed at $z=21\text{cm}$ for $P_i=37$ and 250kW are shown in Fig. 6(a) and Fig. 6(b), when the pulsewidth of the microwave pulse are 1 and $3\mu\text{s}$. The solid line represents the spectrum for incident power $P_i=250\text{kW}$ and the dashed line represents the one for 37kW . It can be seen from Fig. 6 that

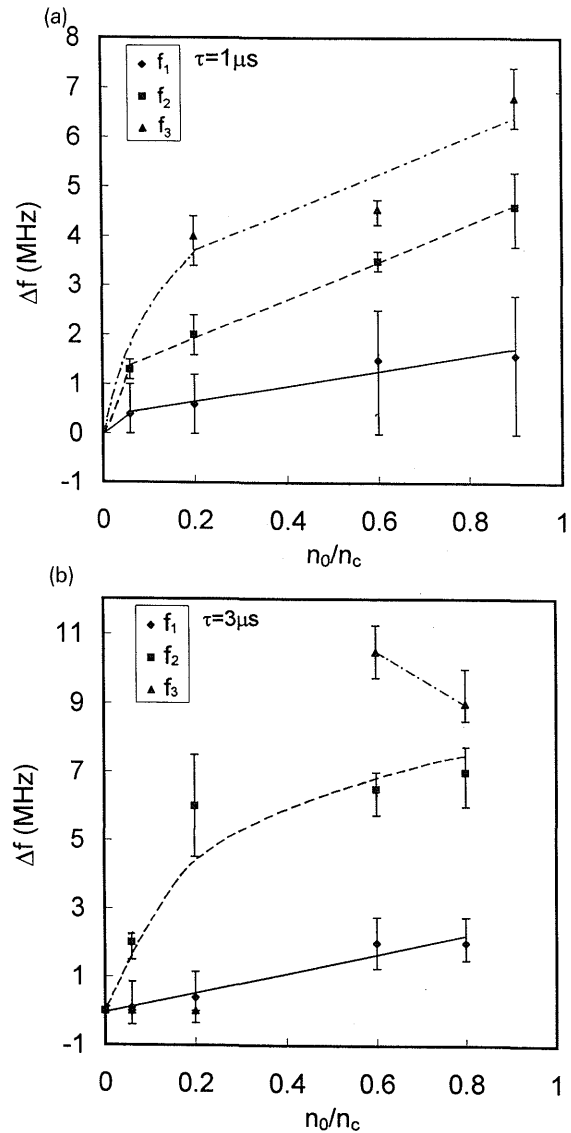


Fig. 5 Frequency up-shifts and new higher frequency components vs. plasma density n_0 . (a) Pulse-width $\tau=1\mu\text{s}$, and (b) $\tau=3\mu\text{s}$. $0.06n_c \leq n_0 \leq 0.8n_c$, $P_i=250\text{kW}$, $P_{Ar}=2 \times 10^{-3}$ Torr, $z=21\text{cm}$ and $z_r=0$.

the higher the incident power the larger the frequency up-shifts and the frequency components in the upper frequency range. Such as in Fig. 6(a), when $P_i=250\text{kW}$, the up-shifted frequency of about 1.5MHz and the higher frequency components of 4.2, 5 and 7.5MHz have been observed, but when $P_i=37\text{kW}$, the frequency up-shift is around 0.5MHz and only one obvious peak of the higher frequency component around 3.5MHz has been observed. The fact that the frequency shifts depend on the incident power directly is clear. The relationship of the frequency shifts and the incident is plotted in Fig. 7. From Figs. 7(a) and (b), we found

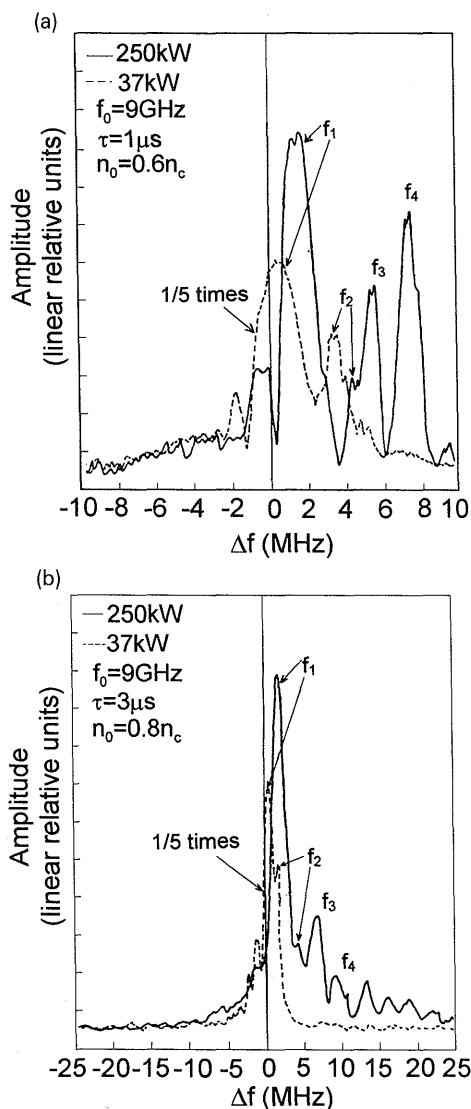


Fig. 6 Typical frequency spectra vs. incident power. (a) Pulse-width $\tau=1\mu\text{s}$, and (b) $\tau=3\mu\text{s}$. Dashed line represents the spectrum observed with $P_i=37\text{kW}$, and solid line represents the case with $P_i=250\text{kW}$. $n_0 \approx 0.6n_c$, $P_{Ar}=2 \times 10^{-3}$ Torr, $z=21\text{cm}$ and $z_r=0$.

that as the incident power of the microwave P_i is increased from 0 to 250kW, the frequency up-shifts (f_1) and the higher frequency components increase almost linearly. Another important thing is that the frequency component which is higher than the center frequency (9GHz) can only be observed when P_i is higher than 7.9kW, *i.e.* the threshold power for the present phenomenon is around 7.9kW.

3.4. Time evolution of the frequency up-shift

As mentioned above, the each frequency spectrum shown in Sections 3.1., 3.2., and 3.3. reflects the aver-

age of the up-shifted frequency and the higher frequency components of 500 microwave pulses. In order to investigate the time evolution of the frequency up-shift and higher frequency components within a pulse-width, the probes are fixed at one point inside the plasma. The incident microwave signal from a directional coupler which is installed in front of the horn antenna and the up-shifted microwave signal picked by the cylindrical probe in the plasma are fed into a mixer. The rf signal observed through the mixer is recorded by

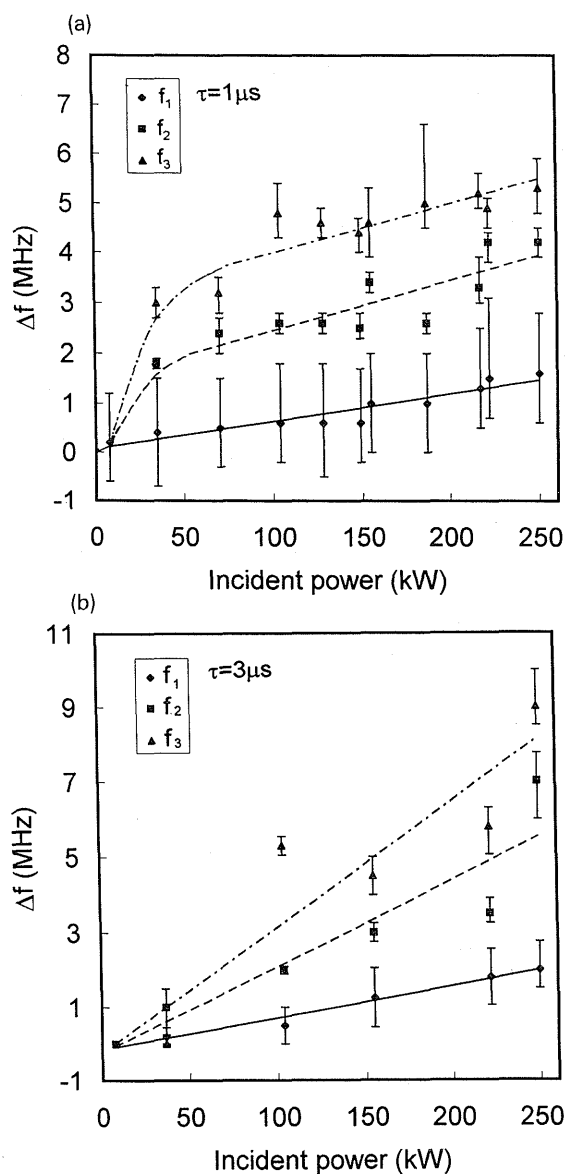


Fig. 7 Frequency up-shift and new higher components vs. incident power P_i . (a) Pulse-width $\tau=1\mu\text{s}$, and (b) $\tau=3\mu\text{s}$. $P_i=7.9\text{kW} \sim 250\text{kW}$, $n_0 \approx 0.6n_c$, $P_{Ar}=2 \times 10^{-3}$ Torr, $z=21\text{cm}$ and $z_r=0$.

the digital storage oscilloscope. At the same time, the microwave pulse and its frequency spectrum are observed by a X'tal and the spectrum analyzer, respectively, so that we can analyze the signal from the mixer and compare the results with the spectrum obtained by the spectrum analyzer.

As an example, the results observed at $z=21\text{cm}$ are shown in Fig. 8 when plasma density is $n_0=0.6n_c$ at this point, incident power is $P_i=250\text{kW}$ and the pulse-width of the incident microwave is $\tau \approx 3\mu\text{s}$. Fig. 8(a) shows the spectrum observed by the spectrum analyzer. Same as before, Fig. 8(a) shows a frequency up-shift (f_1) and higher frequency components from 4 to 25MHz with a continuous background. The peaks, f_1, f_2, f_3, f_4 , in this spectrum are around +2, +5, +14, +21MHz, respectively. By applying a Fast Fourier Transform (sampled at 250MHz with 8-bit resolution) to the signal from the mixer, we obtain the frequency spectrum of one microwave pulse, as shown in Fig. 8(b). For the peaks ($f_1=1.5\text{MHz}$, $f_2=5\text{MHz}$, $f_3=14\text{MHz}$, $f_4=23\text{MHz}$) shown in Fig. 8(b), the corresponding Stokes frequencies can almost be found in Fig. 8(a). It is obvious that all the frequency components shown by the peaks in Fig. 8(b) are contained in Fig. 8(a). This means that the spectrum shown in Fig. 8(b) is one of the representative ones for a microwave pulse experienced frequency up-shift. So that the frequency shift of one incident microwave pulse can be obtained from Fig. 8(b).

In order to investigate the time evolution of the up-shifted frequencies within one microwave pulse, the Fast Fourier Transform is applied again to the rf signal observed by the mixer by subdividing the signal into 16 section of 256ns each on the time window of $4\mu\text{s}$. The result is given in Fig. 8(c). It reflects the time evolution of the frequency up-shift and the higher frequency components shown in Fig. 8(b). In this graph, the brighter the color the higher the amplitude of the corresponding component. It is clear that the frequency and the amplitude of every frequency component increase in time from $0.2\mu\text{s}$ (the beginning of the microwave pulse) to $2.5\mu\text{s}$. But after $t=2.5\mu\text{s}$, the higher frequencies decrease to almost zero. This phenomenon can be explained according to the pulse shape of the microwave signal detected experimentally at $z=21\text{cm}$, as shown in Fig. 8(d). Although the pulsewidth of the incident microwave is $3\mu\text{s}$, the pulsewidth of the signal shown in Fig. 8(d) is $2.5\mu\text{s}$. This is because the incident microwave almost could not be fed into the chamber after $t=2.5\mu\text{s}$ due to the reflected microwave from the chamber wall and the plasma. We also noted that the

$|E|^2$ shown in Fig. 8(d) changes in time which may be resulted from the fluctuation of the plasma density or the reflected wave, and around $t=1\mu\text{s}$ the amplitude of $|E|^2$ is quite low. From Fig. 8(c), we can also see that the frequency shifts and their amplitudes become small near $t=1\mu\text{s}$ and the higher frequency shifts are corresponding to the two high peaks in Fig. 8(c). Consequently, the results obtained above are reasonable and we can conclude that the frequency shifts, higher frequency components and the amplitudes of those frequencies are an obvious function of time.

3.5. Velocity of the plasma flow

Whether the up-shifts of the frequency are related to a moving plasma or not is suspected. Therefore, the velocity of plasma flow has also been measured during the experiment. The density perturbation is observed by the plane probe which is moved step by step along the center axis of the chamber. The density perturbation observed from $z=21\text{cm}$ to 22cm are shown in Fig. 9(a) as an example. The phase delay vs. probe separation from $z=20$ to 21cm and $z=21$ to 22cm are plotted in Fig. 9(b) separately. The numbers 1 and 2 represent the first and second peaks of the density perturbation after turn-off of the microwave pulse, as shown partly in Fig. 9(a). It can be seen from Fig. 9(b) that the plasma expands towards two directions from $z \approx 21\text{cm}$ with a velocity of $v \approx 1.0 \times 10^6\text{cm/s}$, in this example. This velocity is almost 4 times of $c_s \approx 2.5 \times 10^5\text{cm/s}$, the velocity of ion acoustic wave in our case. As mentioned above, in the present experiments, we found that the electric field intensity $|E|^2$ has a standing wave structure in space because of the reflection from the plasma and the end wall of the chamber (see Fig. 1(a)). And, there is a very high peak of the electric field intensity at $z \approx 21\text{cm}$ as shown again by the dotted line in Fig. 9(b). Because of this strong electric field the plasma is pushed away from this point towards two directions by a ponderomotive force. Then, the moving plasma is created by the ponderomotive force of the standing wave.

3.6. Relationship of frequency spectra and the reflecting position of the microwave

According to the results given in Section 3.5., the plasma flows with a quite high speed are created at the place where the peak of the standing wave is very high. In the present experiments, the obvious frequency shifts and the higher frequency components are observed around $z=11$ and 21cm . It seems that the frequency up-shift is related to the value of the electric field

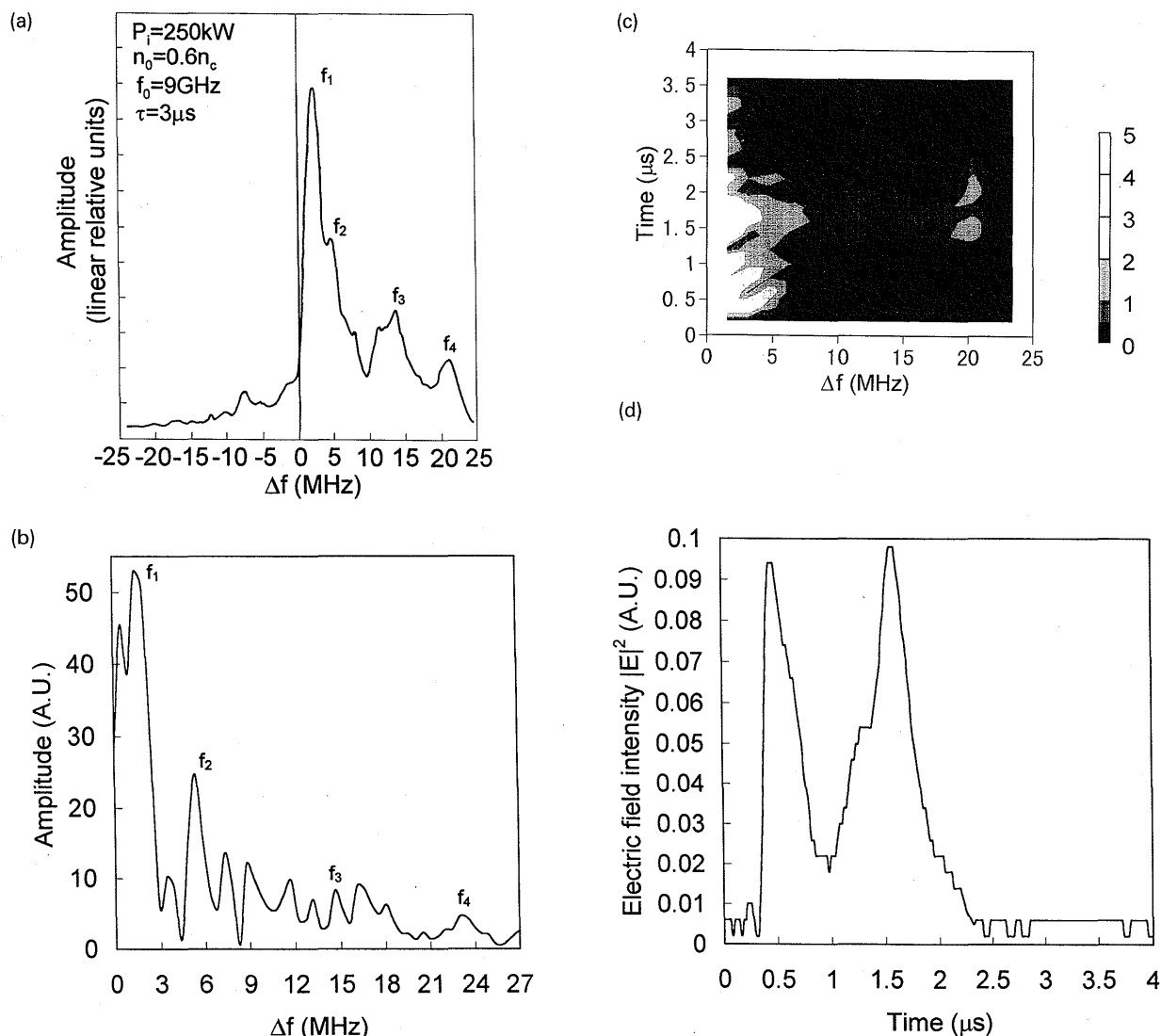


Fig. 8 Comparison of frequency spectra. (a) Frequency spectrum observed by a spectrum analyzer, (b) Frequency spectrum obtained by applying a FFT to a signal from a mixer, (c) Time evolution of frequency up-shift and higher frequency components, and (d) microwave pulse in the plasma. $P_i=250\text{kW}$, $\tau=3\mu\text{s}$, $n_0 \approx 0.6n_c$, $P_{Ar}=2 \times 10^{-3}$ Torr, $z=21\text{cm}$ and $z_r=0$.

intensity directly. In order to investigate the dependence of frequency spectra on the intensity of the electric field, a moveable reflecting plate is put near the end wall of the chamber ($z_r=0\text{cm}$). By changing the position of this reflecting plate, the electric intensity measured at a fixed point should be changed.

The electric field intensity of the incident wave $|E|^2$ and frequency spectra are observed at the same time at the point $z=21\text{cm}$ while the reflecting plate is moved from $z_r=0$ to 9cm with a step $\Delta z_r=0.4\text{cm}$. The electric field intensity, the frequency up-shift and higher frequency components at $z=21\text{cm}$ as the function of the position of the reflecting plate are shown in Fig. 10(a) and (b), respectively. Comparing these results, we

note that at the positions the high peaks of the electric field intensity are observed, the frequency up-shifts and the higher frequency components are detected. So that we can conclude that the stronger the intensity of the electric field, the higher the frequency up-shifts and higher frequency components.

4. Theoretical Model

In the previous experiments of laser (or microwave)-plasma interaction, frequency shifts, especially the down-shifts (red-shifts), have been observed, such as in the experiments of stimulated Brillouin scattering (SBS) [1,2] and stimulated Raman scattering (SRS) [13]. In laser produced plasma, the up-shifted scattered

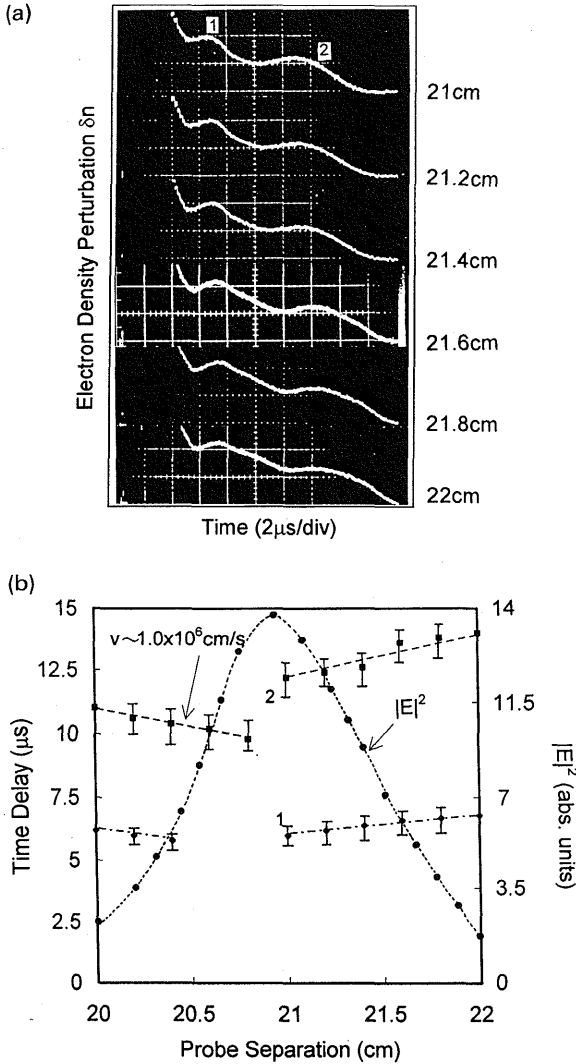


Fig. 9 Measured velocity of plasma flow. (a) Examples of electron density perturbation observed around $z=21$ cm. (b) Time-space display of the plasma flow. $n_0 \approx 0.6n_c$ at $z=21$ cm, $P_i=250$ kW, $\tau \approx 1\mu$ s, $P_{Ar}=2 \times 10^{-3}$ Torr and $z_r=0$.

light can result from the hydrodynamic expansion of the plasma due to the ablation of the target [14]. Nevertheless, the ablation of the target is impossible in our case. Of course, when the oscillating two-stream instability occurs, the up-shifted frequency components which are dominant in the spectra have been observed [15]. However, the up-shifted components are around $3\omega_0/2$. A frequency up-shift about 1.5MHz had been observed in Ref. [16] when a microwave pulse interacted with a rapidly growing plasma in which there was a temporal growing ionization front. But in the present experiments there is no ionization front or temporal plasma density growing during the interaction of the

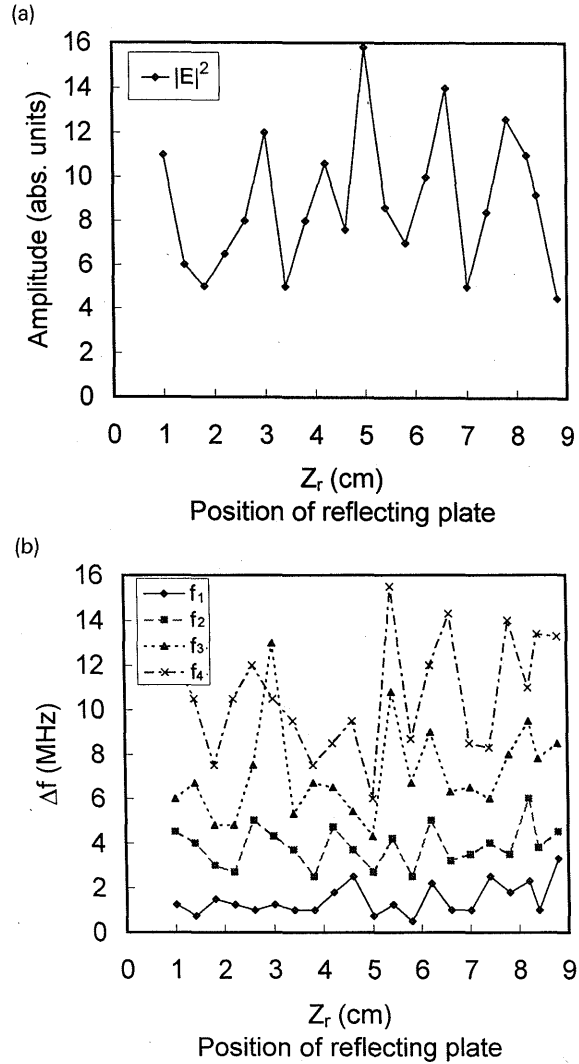


Fig. 10 (a) Electric field intensity at $z=21$ cm vs. the position of the reflecting plate z_r . (b) Higher frequencies f_1 , f_2 , f_3 and f_4 vs. the position of the reflecting plate z_r . $n_0 \approx 0.6n_c$ at $z=21$ cm, $P_i=250$ kW, $\tau \approx 3\mu$ s, and $P_{Ar}=2 \times 10^{-3}$ Torr.

microwave and plasma. So, neither the theories in Refs. [5-10], nor the two-stream instability can explain the phenomena in our experiments.

As mentioned above, it is obvious that the up-shifted frequency and higher frequency components observed in the present experiments depend not only on the incident microwave power and plasma density but also on where the signal is detected. Another thing which should be also noted is that the plasma flow propagates at very high speed and the frequency spectrum depends on the strength of the electric field intensity directly. In our case, because an inhomogeneous standing wave with two very high peaks is built in the chamber

along the center axis, there is a ponderomotive force which reverses sign in each striation. The plasma can be expanded at a very high speed by the ponderomotive force, then a moving plasma can be resulted. Consequently, during the incident wave interacts with the moving plasma, the frequency is up-shifted due to Doppler effect.

4.1. Moving plasma

A typical spatial pattern of an electric field intensity $|E|^2$ along chamber axis and the resulted moving plasma are shown in Fig. 11. For simplicity, we only consider the moving plasmas at the two sides of one very high peak of the electric field intensity $|E_1|^2$. As shown in Fig. 11, because of the electric field intensity $|E_1|^2 \gg |E_2|^2, |E_3|^2$, then the velocities of the moving plasmas with the relationship $v_1 \gg v_2, v_3$ can be assumed. Therefore, the main effect of the frequency up-shift come from the moving plasmas with the velocity v_1 .

In order to estimate the up-shifted frequency due to the Doppler effect theoretically, first we should calculate the speed of the moving plasma. The ponderomotive force acting on the plasma can be written as [17]

$$F_{NL} = -\frac{\epsilon_0 \omega_p^2}{\omega^2} \nabla \frac{\langle E^2 \rangle}{2} \approx \frac{\omega_p^2}{\omega^2} \frac{\epsilon_0 \langle E^2 \rangle}{2l}, \quad (1)$$

where $\omega_p = (n_0 e^2 / \epsilon_0 m_e)^{1/2}$ is the plasma frequency and l is the gradient scale length of $\langle E^2 \rangle$. The pressure-gradient force in the plasma is

$$F_{\text{pressure}} = -\nabla p = -K(T_i + T_e) \nabla n_0. \quad (2)$$

where, T_i and T_e are ion temperature and electron temperature, respectively. Using Eqs. (1), (2) and the equation of motion for the plasma, we find the speed of the expanding plasma is

$$v \approx \left[\frac{4P_i}{cA} \frac{\omega_p^2}{\omega^2} - K(T_i + T_e) \nabla n_0 \right] \tau / (m_i n_0), \quad (3)$$

where A is the irradiation area of the microwave. c is the speed of light in vacuum and m_i is ion mass. If we take $P_i = 250\text{kW}$, $f_0 = 9\text{GHz}$, $T_e = 3\text{eV} \gg T_i \approx 0.3\text{eV}$, $A = 6 \times 10^{-4}\text{m}^2$, $\tau = 1\mu\text{s}$, $l = 8 \times 10^{-3}\text{m}$, the speed of the expanding plasma is $v \approx 1.1 \times 10^6\text{cm/s}$. When the pulsewidth of the incident microwave is $\tau = 3\mu\text{s}$, $v \approx 3.3 \times 10^6\text{cm/s}$.

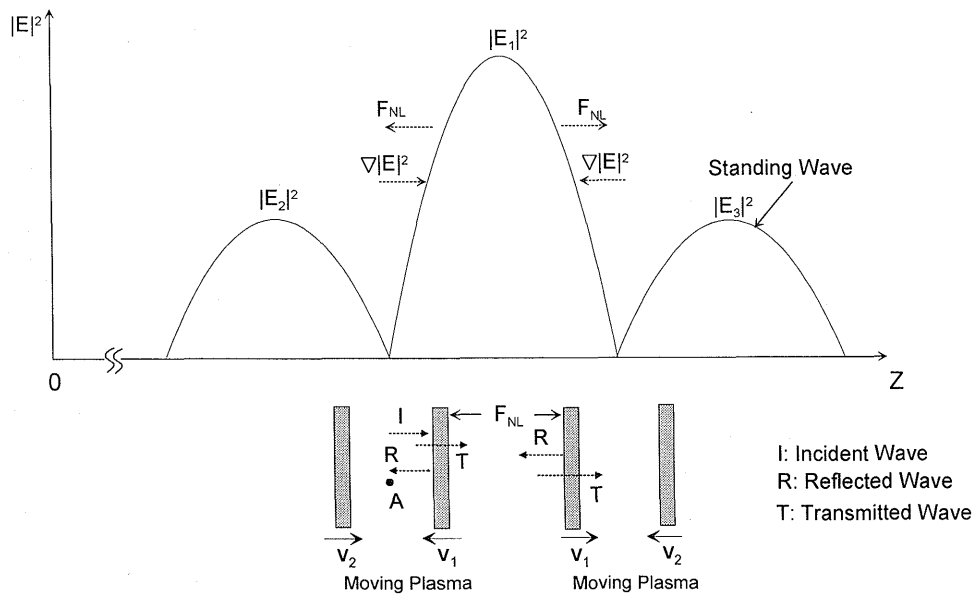


Fig. 11 Spatial pattern of an electric field intensity along the chamber axis, and the moving plasmas arising from the ponderomotive force of an electric field. $|E_m|^2$ ($m=1,2,\dots$) is corresponding to the peak of the standing wave. v_m ($m=1,2,\dots$) is the velocity of the moving plasma. R is reflection coefficient and $T=1-R$ is transmission coefficient.

4.2. Frequency up-shift by a moving plasma

As discussed above, a moving plasma is created by the strong standing wave in the chamber. When the incident wave encounters such a moving plasma, a part of it is reflected by the plasma and the rest is transmitted through the moving plasma. When the moving plasma is traveling at speed v , then by applying a Lorentz transforming to laboratory frame the incident wave frequency and wave number in the frame of the moving plasma (the primed frame) are obtained as follows [18]

$$\omega'_0 = \gamma(1 + \beta)\omega_0, \quad (4)$$

$$k'_0 = \gamma(1 + \beta)k_0, \quad (5)$$

where $\gamma=(1-\beta^2)^{-1/2}$, $\beta=v/c$. In this frame the wave is reflected at a stationary boundary, thus

$$\omega'_r = \omega'_0, \quad (6)$$

$$k'_r = -k'_0. \quad (7)$$

Performing an inverse Lorentz transformation to get back to the laboratory frame, the wave frequency and wave number for the reflected wave are

$$\omega_r = \gamma^2(1 + \beta)^2\omega_0, \quad (8)$$

$$k_r = -\gamma^2(1 + \beta)^2k_0, \quad (9)$$

while for the transmitted wave, it is found that [19]

$$\omega_t = \gamma^2(1 + \beta) \left[1 - \beta \left(1 - \frac{\omega_p^2}{\omega_0^2 \gamma^2 (1 + \beta)^2} \right)^{\frac{1}{2}} \right] \omega_0, \quad (10)$$

$$k_t = \gamma^2(1 + \beta) \left[\left(1 - \frac{\omega_p^2}{\omega_0^2 \gamma^2 (1 + \beta)^2} \right)^{\frac{1}{2}} - \beta \right] k_0. \quad (11)$$

For the incident microwave with pulsewidth $\tau=1\mu\text{s}$, by substituting $v=1.1 \times 10^6\text{cm/s}$ into Eq. (8) the frequency up-shift of the reflected wave due to the Doppler effect is obtained as

$$\Delta f_r = \frac{2\beta f_0}{1 - \beta} = 0.7(\text{MHz}), \quad (12)$$

and for the transmitted wave, from Eq. (10) the frequency up-shifted is

$$\Delta f_t = \frac{\beta f_0}{1 - \beta} = 0.4(\text{MHz}), \quad (13)$$

because of $\beta \ll 1$ in the present experiments. For $\tau=3\mu\text{s}$, the $\Delta f_r=2.1\text{MHz}$ and $\Delta f_t=1.2\text{MHz}$, respectively. These results are in good agreement with the experimental results. As shown in Fig. 10, the speed of

the plasma flow is around $1 \times 10^6\text{cm/s}$. According to this value, the Δf_r and Δf_t are 0.5MHz and 0.3MHz, respectively. But this velocity of the plasma flow is observed after the rf pulse. During the rf pulse, the speed of the moving plasma may be higher.

Since the up-shifted frequency signals would interact with the moving plasma several times within one pulsewidth of the incident microwave, it is a possible reason that why the higher frequency components have been observed in our experiments. The frequency spectrum of the rf signal observed in the present experiments is the sum of the up-shifted reflected and transmitted waves.

Of course, the frequency down-shifts can also be resulted by the reflection of the moving plasma in the present experiments. As shown in Fig. 11, if a measurement is taken at point A, the amplitude of up-shifted frequency signals due to the reflection of the moving plasma can be written as

$$|E|_{\text{up-shift}} = R|E_0|(\Delta\omega) + R^2|E_0|(2\Delta\omega) + R^3|E_0|(3\Delta\omega) + \dots, \quad (14)$$

while the down-shifted one is

$$|E|_{\text{down-shift}} = R(1 - R)^2|E_0|(-\Delta\omega) + \dots, \quad (15)$$

where R is reflection coefficient and $\Delta\omega$ is fundamental frequency up-shift. For example, when $R \approx 0.5$, the amplitudes of the up and down shifts signals are $|E|_{\text{up-shift}} \approx 0.8|E_0|$ and $|E|_{\text{down-shift}} \approx 0.1|E_0|$, respectively, according to Eqs. (14) and (15). The amplitude of the down-shifted frequency signal is much smaller than that of up-shifted one. So in the present experiments, we can not distinguish it in the frequency spectra. As shown in Eq. (14), the higher frequency components such as $R^2|E_0|$ for $2\Delta\omega$, $R^3|E_0|$ for $3\Delta\omega$ and so forth can be expected. Here the fundamental frequency up-shift is $\Delta\omega$, as obtained in Eq. (12) theoretically. These results are quite similar to that of in the experiments (see Fig. 3(a) or 3(b)). Furthermore, because of the expanding plasma is a shock wave, at a point where the electric field is very strong, the local density may be much higher than the average plasma density. So, a total reflection ($R=1$) from this point is possible. Then at this local point, the up-shift due to the reflection is dominant. As mentioned before, the observed higher frequency components may result from the multi-reflection and multi-transmission through the moving plasma(s). But about the validity of this interpretation, it is not clear until now. Further experimental investigation and theoretical calculation are necessary.

5. Conclusions

In summary, the frequency up-shift around 1.0~2MHz and some other higher frequency components in the range of 3MHz to 23MHz have been observed in our experiments. This is the first time that the frequency up-shift (blue-shift) being demonstrated in the experiments of microwave-plasma interaction when there is no ionization in the plasma. The frequency up-shifts and higher frequency components have been found to be proportional to the plasma density and incident power. The dependence of the frequency spectra on the spatial position, or in the other words, on the intensity of the electric field at that position have also been verified clearly. The threshold value of incident power around 7.9kW has been found, and the time evolution of the frequency spectrum also shows that the longer the interaction time, the higher the frequency up-shifts.

In the present experiments, because a very strong standing wave is established in the chamber, the plasma is expanded rapidly by the collective ponderomotive force arising from the electric field gradient of the standing wave. The frequency of the incident wave is up-shifted due to the Doppler effect resulting from the moving plasma. The experimental results are in good agreement with the results of the theoretical calculations.

Frequency up-shifts and pulse compression which are possible for underdense relativistic ionization fronts have been predicted [10] and proved successfully [11,12]. The phenomenon observed in the present experiments shows that not only an ionization front but also an underdense moving plasma can be used to up-shift an electromagnetic radiation. This phenomenon is of relevance to the field of laser-plasma interactions because it may happen in the experiments of laser-plasma interaction also. Our results also show that a careful diagnosis is necessary when the experiment of laser (microwave)-plasma interaction related to a frequency shift is carried out, in order to pinpoint the mechanism of the frequency shift.

Acknowledgments

We would like to thank Mr. H. Itoh for his cooperation on setting the experimental apparatus up. One of the authors, Xu, would like to acknowledge useful discussions with Mr. T. Ueiki also. This work is supported by a Grant-in-Aid for Science Research from Ministry of Education, Science, Sports and Culture of Japan.

References

- [1] S. H. Batha *et al.*, Phys. Rev. Lett. **70**, 802 (1993).
- [2] L. V. Powers *et al.*, Phys. Rev. Lett. **74**, 2957 (1995).
- [3] W. L. Kruer, *The Physics of Laser Plasma Interactions*. Addison-Wesley, New York, 1988.
- [4] M. N. Rosenbluth and R. Z. Sagdeev, *Handbook of Plasma Physics, Volume 3*, North-Holland, New York, 1991.
- [5] S. C. Wilks, J. M. Dawson, W. B. Mori, T. Katsouleas and M. E. Jones, Phys. Rev. Lett. **62**, 2600 (1989).
- [6] P. Sprangle, E. Esarey and A. Ting, Phys. Rev A **41**, 4463 (1990).
- [7] E. Esarey, G. Joyce and P. Sprangle, Phys. Rev A **44**, 3908 (1991).
- [8] E. Yablonovitch, Phys. Rev. Lett. **31**, 877 (1975); **32**, 1101 (1974).
- [9] M. Lampe, E. Ott and J. H. Walker, Phys. Fluids **10**, 42 (1978).
- [10] W. B. Mori, Phys. Rev. A **44**, 5118 (1991).
- [11] W. M. Wood, C. W. Siders and M. C. Downer, Phys. Rev. Lett. **67**, 3523 (1991); W. M. Wood, C. W. Siders and M. C. Downer, IEEE Trans. Plasma Sci. **21**, 20 (1993).
- [12] R. L. Savage, R. P. Brogle, W. B. Mori, and C. Joshi, IEEE Trans. Plasma Sci. **21**, 5 (1993); R. L. Savage, Jr., C. Joshi, and W. B. Mori, Phys. Rev. Lett. **68**, 946 (1992).
- [13] M. J. Everett *et al.*, Phys. Rev. Lett. **74**, 1355 (1995).
- [14] D. W. Phillion, W. L. Kruer and V. C. Rupert, Phys. Rev. Lett. **39**, 1405 (1977).
- [15] P. E. Young *et al.*, Phys. Rev. Lett. **61**, 2766 (1988).
- [16] S. P. Kuo, Phys. Rev. Lett. **65**, 1000 (1990).
- [17] F. F. Chen: *Introduction to Plasma Physics and Controlled Fusion, Volume 1: Plasma Physics*, Plenum, New York (1984).
- [18] J. D. Jackson, *Classical Electrodynamics*, Second Edition, Wiley, New York, 1975.
- [19] R. P. Brogle, *Research Reports of UCLA, PPG-1463*, September 1992.